

Performance of WRF Large Eddy Simulations in Modeling the Convective Boundary Layer over the Taklimakan Desert, China

Hongxiong XU¹, Minzhong WANG^{1,2,4*}, Yinjun WANG¹, and Wenyue CAI^{1,3}

¹ State Key Laboratory of Severe Weather, Chinese Academy of Meteorological Sciences, Beijing 100081

² Institute of Desert Meteorology, China Meteorological Administration, Urumqi 830002

³ National Climate Center, China Meteorological Administration, Beijing 100081

⁴ Taklimakan Desert Atmospheric Environment Observation Experimental Station, Tazhong 841000

(Received January 2, 2018; in final form September 11, 2018)

ABSTRACT

The maximum height of the convective boundary layer (CBL) over the Taklimakan Desert can exceed 5000 m during summer and plays a crucial role in the regional circulation and weather. We combined the Weather Research and Forecasting Large Eddy Simulation (WRF-LES) with data from Global Positioning System (GPS) radiosondes and from eddy covariance stations to evaluate the performance of the WRF-LES in simulating the characteristics of the deep CBL over the central Taklimakan Desert. The model reproduced the evolution of the CBL processes reasonably well, but the simulations generated warmer and moister conditions than the observation as a result of the over-prediction of surface fluxes and large-scale advection. Further simulations were performed with multiple configurations and sensitivity tests. The sensitivity tests for the lateral boundary conditions (LBCs) showed that the model results are sensitive to changes in the time resolution and domain size of the specified LBCs. A larger domain size varies the distance of the area of interest from the LBCs and reduces the influence of large forecast errors near the LBCs. Comparing the model results using the original parameterization of sensible heat flux with the Noah land surface scheme and those of the sensitivity experiments showed that the desert CBL is sensitive to the sensible heat flux produced by the land surface scheme during daytime in summer. A reduction in the sensible heat flux can correct overestimates of the potential temperature profile. However, increasing the sensible heat flux significantly reduces the total time needed to increase the CBL to a relatively low altitude (< 3 km) in the middle and initial stages of the development of the CBL rather than producing a higher CBL in the later stages.

Key words: Weather Research and Forecasting Model (WRF), Large Eddy Simulation (LES), convective boundary layer (CBL), the Taklimakan Desert

Citation: Xu, H. X., M. Z. Wang, Y. J. Wang, et al., 2018: Performance of WRF Large Eddy Simulations in modeling the convective boundary layer over the Taklimakan Desert, China. *J. Meteor. Res.*, **32**(6), 1011–1025, doi: 10.1007/s13351-018-8001-1.

1. Introduction

The Taklimakan Desert in southern-central Xinjiang Autonomous Region, China, is the world's second-largest flow desert and has a profound influence on the regional weather and climate. As a result of the extreme variation of near-surface temperatures, the planetary boundary layer (PBL) in this region commonly reaches 4–6 km in height during boreal summer, which is the deepest on the earth. The deep PBL, which is significantly higher than that over the surrounding mountains

and oases, plays an important role in the regional circulation and weather. Accurate forecast of PBL processes over the Taklimakan in Northwest China Desert is an important task.

The atmosphere over large deserts (such as the Sahara and Taklimakan deserts) is a key component in the earth's climate system. Surface heating from intense solar radiation leads to the development of a near-surface, low-pressure thermal system, commonly referred to as a heat low (Engelstaedter et al., 2015). However, despite the vital role that deserts have in the earth's climate system,

Supported by the National Natural Science Foundation of China (41575008 and 41775030).

*Corresponding author: wangmz@idm.cn.

©The Chinese Meteorological Society and Springer-Verlag Berlin Heidelberg 2018

observations are extremely sparse, and the available data are usually obtained from surrounding areas (Marsham et al., 2011). This lack of observational data has restricted the development of our understanding of deserts and has led to large discrepancies in analyses and significant biases in operational numerical weather prediction (NWP) models. The ability of local models to simulate real-world examples is often hindered by a lack of data with which to assess the performance of the model (Garcia-Carreras et al., 2015).

To fill in the gaps in the available data for the Taklimakan Desert, a field observation experiment was carried out during July 2016 in Tazhong, located in the center of the Taklimakan Desert near the Institute of Desert Meteorology, Chinese Meteorological Administration, at Urumqi (Liu et al., 2012; Wang et al., 2016a, b). These data will allow the evaluation of the performance of the deep PBL process in NWP models over the Taklimakan Desert.

The motion of the atmosphere interweaves small-scale, complex interactions with multiscale nonlinear interactions. As a result of their limited resolution in both time and space, mesoscale atmospheric models are unable to represent all these processes (Talbot et al., 2012), which include turbulent motion on a scale that is too small to be resolved by simplified processes in atmospheric models. Turbulent mixing throughout the PBL can have a large impact on forecasts by NWP models (Shin and Hong, 2011, 2015).

Complex turbulent flows in NWP models can be analyzed by large eddy simulation (LES) techniques, which can explicitly resolve the energy-containing turbulent motions responsible for turbulent transport (Moeng et al., 2007). LES techniques have been used intensively to examine the detailed structure of turbulence, to generate statistics and to study physical processes (Sun and Xu, 2009; Heinold et al., 2013, 2015; Garcia-Carreras et al., 2015; Heinze et al., 2015). However, most applications of LES techniques to the PBL have been limited to idealized physical conditions. Recently, some studies have attempted to test and assess the performance of LES in simulating real-world case studies (Liu et al., 2011; Talbot et al., 2012). Liu et al. (2011) suggested that the Weather Research and Forecasting Large Eddy Simulation (WRF-LES) is a valuable tool with which to simulate real-world microscale weather flows and to develop real-time forecasting systems, although further modeling to determine the accuracy of synoptic forcing and the effect of resolution has been highly recommended. Talbot et al. (2012) suggested that the ability of WRF-LES to

simulate real-world examples is hindered by a lack of favorable synoptic forcing. The initial and lateral boundary conditions (LBCs) were found to be more important in the LES results than subgrid-scale turbulence closures. Thus, the LBCs can significantly alter the status of high-resolution LESs via inflow boundaries (Rai et al., 2017).

Most of the LES research over desert regions has been limited to idealized physical conditions (Garcia-Carreras et al., 2015) or conducted outside the Taklimakan Desert (Liu et al., 2011; Talbot et al., 2012). The aim of this study is to apply LES to a real example of a deep convective boundary layer (CBL) over the Taklimakan Desert. An important aspect of this study is to assess the skillfulness of the WRF-LES in simulating real examples of deep desert PBL processes at a relatively coarse resolution (333 m) over the Taklimakan Desert during the boreal summer. We first use a combination of the Global Positioning System (GPS) radiosonde and surface fluxes over the central Taklimakan Desert calculated by using an eddy covariance method to evaluate the performance of the WRF-LES in a real-world example. We then assess the potential errors related to the LBCs. One of our aims is to evaluate the relative contribution of uncertainties in the surface model to the typical behavior of PBL processes by conducting sensitivity experiments. We therefore study the sensitivity of the model performance to the surface sensible heat flux. Section 2 gives a brief description of the synoptic conditions of the case study and describes the data, model configuration, and design of the numerical experiments. The results of the numerical simulations are presented in Section 3 and our conclusions are summarized in Section 4.

2. Methods

2.1 Model configuration

We used version 3.8.1 of the WRF model (Skamarock et al., 2008) at a sub-kilometer resolution to simulate an extreme CBL over the Taklimakan Desert. The model is integrated for 12 h, starting from 0800 BT (Beijing Time) 1 July 2016. We use one-way nested WRF model from the mesoscale down to LES scales. All the domains consist of 51 levels extended to 50 hPa. The altitudes for the lowest 20 levels are 1130, 1157, 1207, 1294, 1423, 1591, 1795, 2021, 2272, 2558, 2882, 3248, 3658, 4118, 4633, 5212, 5855, 6517, 7151, and 7757 m ASL (above sea level) and the horizontal spacings of the model are 12, 3, 1, and 0.33 km for D01, D02, D03, and D04. We used 411×321 , 791×651 , 211×201 , and 403×406 model grids. Figure 1 shows the domain used for all the

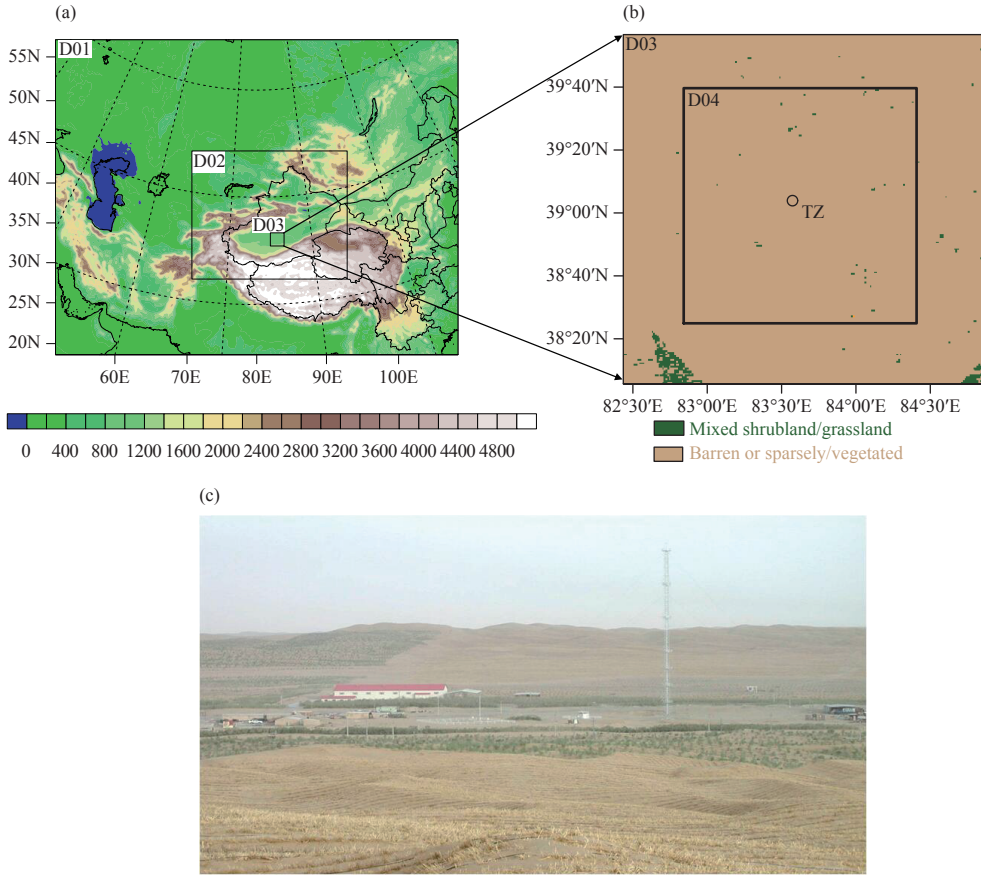


Fig. 1. Simulation domains used in the ARW model with (a) the terrain height (shaded; m), (b) the land use categories for domains D03 and D04, and (c) photograph of the area around Tazhong station.

experiments except BDY_T3. A smaller grid size (205×208) is used in experiment BDY_T3 to verify the effect of domain size on the LES.

The initial and LBCs are provided at the coarsest mesoscale simulations from the NCEP Global Data Assimilation System Final Operational Global Analyses dataset. The analyses are $0.25^\circ \times 0.25^\circ$ grids operationally prepared every six hours and available on the surface and at 32 mandatory (and other pressure) levels from 1000 to 10 hPa (National Centers for Environmental Prediction et al., 2015).

The physical options in the model include the WSM5 microphysics scheme (Hong and Lim, 2006), the Yonsei University PBL scheme (Hong and Pan, 1996), the Kain–Fritsch cumulus parameterization scheme (Kain and Fritsch, 1993; Kain, 2004), the rapid update cycle (RUC) land surface model (Smirnova et al., 1997, 2000), the rapid radiative transfer model (Mlawer et al., 1997) at long wavelengths, and the Dudhia shortwave radiation scheme (Dudhia, 1989). The cumulus parameterization scheme is only applied to the D01 (12 km) grid domain to parameterize the convective rainfall and the LES is only applied to D04 (0.333 km).

Table 1 lists the experiments. Experiment 1 was the control experiment, denoted as CTRL. Experiments 2 (6-h updated LBC; denoted BDY_T2) and 3 (with domain sizes 205×208 ; denoted BDY_T3) were conducted as in the CTRL experiment, but with different domain sizes and frequency of LBC updates. In experiments 4 (HFX_%75) and 5 (HFX_%125), the sensible heat flux was reduced and increased to 75% and 125%, respectively, of that in the CTRL experiment in the RUC land surface scheme to highlight the impact of the sensible heat flux on the deep CBL in the Taklimakan Desert. In experiment 6 (denoted Noah), the Noah land surface model (Chen and Dudhia, 2001a, b) replaced the RUC land surface model in the CTRL experiment to discriminate the influence of different land surface models on the deep CBL.

2.2 Data

The model simulations are compared with the Tazhong field experiment carried out throughout the month of July 2016 by the Institute of Desert Meteorology, Chinese Meteorological Administration, at Urumqi. The main station was located at 39.03°N , 86.63°E . The

Table 1. List of designed experiments

Experiment	Name	Remark
1	BDY_T1 (CTRL)	LBC of D04 is provided by D03 every 1 h with 403×406 model grids
2	BDY_T2	As BDY_T1, but LBC of D04 is provided by D03 every 6 h
3	BDY_T3	As BDY_T2, but with 205×208 model grids
4	HFX_%75	As CTRL_T2, but with a sensible heat flux of 75%
5	HFX_%125	As CTRL_T2, but with a sensible heat flux of 125%
6	Noah	As CTRL_T2, but with the Noah land surface model

location is relatively flat with few hills and is covered by sand combined with grass (Fig. 1c). The deep PBL in our simulation was under a cloudless sky in a dry environment.

The surface fluxes were measured by an eddy correlation system using an R3-50 supersonic anemometer developed by Gill (UK) deployed at a height of 10 m. The frequency of data acquisition was 20 Hz and the surface sensible heat flux was calculated by the eddy covariance method.

The vertical profiles were measured by using soundings. Upper air soundings of the temperature, pressure, humidity, and wind speed and direction were conducted three to six times per day with the CASIC23 GPS sounding system developed by the No. 23 Institute of China

Aerospace Science & Industry. The sounding times were 0115, 0715, 1015, 1315, 1615, and 1915 BT.

2.3 Synoptic patterns

Figure 2 shows the synoptic patterns at 0800 BT 1 July 2016 at 850, 700, 500, and 100 hPa. There were cyclonic vortexes from 850 to 500 hPa centered at 55°N (Figs. 2a, b, c). The Taklimakan Desert was located east of the cyclonic vortex and embedded in an east–west elongated ridge at 0800 BT 1 July 2016. To the southwest, influenced by the South Asian high centered over eastern Iranian Plateau, the upper air over the Taklimakan Desert was controlled by the westerly jet stream at 100 hPa (Fig. 2d). A low-pressure system at low levels termed a heat low (Fig. 3), dominated most of southern Xinjiang, and

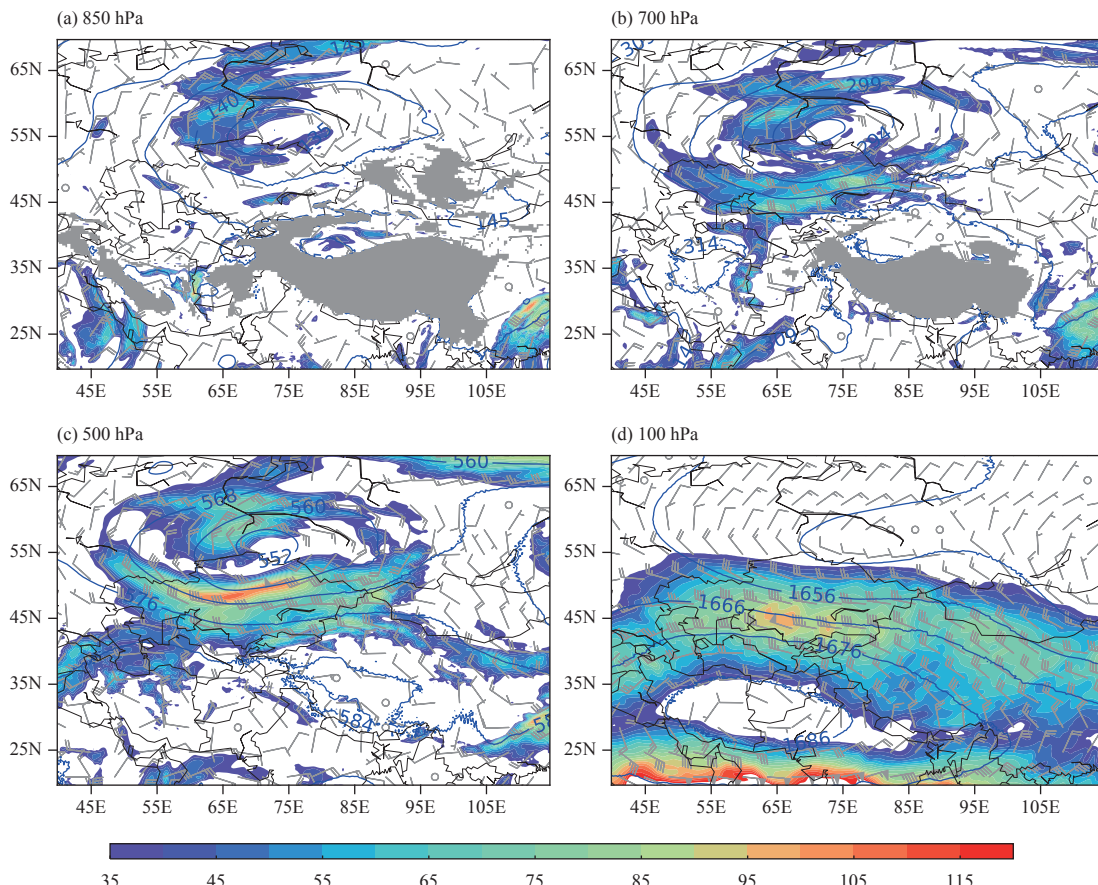


Fig. 2. Horizontal distribution of the geopotential height (solid lines; dagpm), wind speed (shaded; knots), and wind bars from the NCEP FNL analysis at 0800 BT 1 July 2016 at (a) 850, (b) 700, (c) 500, and (d) 100 hPa.

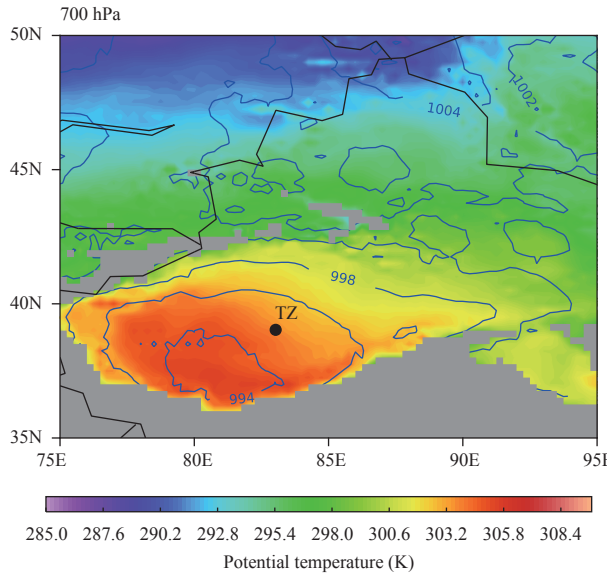


Fig. 3. NCEP FNL 700-hPa potential temperature (colors) and mean sea level pressure (blue lines) at 0800 BT 1 July 2016. The black dot shows the location of Tazhong station in Xinjiang Autonomous Region.

resulted in continuous high temperatures over the desert. This situation favored subsidence and served as a triggering mechanism for the deep PBL in the region in the subsequent two to three days (figure omitted).

3. Results

3.1 Validation of the deep CBL structure

The time series of the surface variables at Tazhong station from the CTRL simulation for 1 July 2016 are presented in Figs. 4a, b. The results show that there are large discrepancies in the thermodynamic surface variables (surface temperature and the sensible and latent heat fluxes) between the model and observations. The surface sensible heat flux is far lower in the observations (maximum 243 W m^{-2}) than in the model (maximum 613 W m^{-2}), indicating that the sensible heat flux from the WRF simulation is 2.5 times than that of the observations when they are both at their maximum. By contrast, the model shows a significant cold bias for the surface temperature, which is much higher in the observations (maximum 70°C) than in the model (maximum 50°C). To further verify the surface variables, the root-mean-square error (RMSE) and mean bias (BIAS) are calculated including integration hours from 3 to 12 h for Tazhong station (Table 2). The model significantly overestimates the sensible heat flux (RMSE 263 W m^{-2} and BIAS 250 W m^{-2}) and dramatically underestimates the surface temperature (RMSE 14°C and BIAS -13°C).

There are two possible reasons for the model sensible heat flux being far greater than that of the observations.

First, there are mismatches in land use between the model and observations. The WRF model is applied land-use categories to assign static parameters and initial values to each grid cell (e.g., the albedo and surface roughness; Schicker et al., 2016). However, Fig. 1c shows that station EC (eddy covariance) is surrounded by a mixture of grass and sand. This complex underlying surface may not be adequately reproduced by the model and may have an impact on the overestimation of the sensible heat flux. Second, the sensible heat flux and the latent heat flux based on the eddy correlation method may be underestimated (LeMone et al., 2013). It has been shown that if the other two terms in the budget (the net radiation and flux into the soil) are accurate, then the data used for the whole experiment to find the sensible and latent heat fluxes for Tazhong station are, on average, 75% of the values required to balance the surface energy budget.

In contrast with the large differences in the surface variables between the model and observations, the near-surface variables (the 2-m temperature, the relative humidity, and the 10-m wind speed in Figs. 4e, f, g) in the model are higher than in the observations. The time series evolution of the 2-m temperatures follow those of the observations (RMSE 1.66 and BIAS 1.61), but the model produces a surface warmer by about 3 K at the beginning of integration and 1 K when the model and observations both reach their maximum temperature.

The results indicate that the near-surface relative humidity in the model is close to the initial observations (Fig. 4f). However, the humidity in the model increases during the first few hours of model integration, while the observed humidity decreases. After 3 h of spin-up, the model reproduces the evolution of humidity reasonably well, in agreement with the observations (RMSE 1.22%), but the values are higher than the observed values (BIAS 1.11%).

One reason for this discrepancy is the overestimation of the soil moisture content during the simulation. The soil moisture content can have a strong influence on the near-surface humidity. An overestimation of the soil moisture content in the initial condition of the model may result in a considerable difference in the humidity of the near-surface layer (Talbot et al., 2012). In our simulations, the model produces large overestimates of the soil moisture content at the first 3-h simulation. At initialization of the model in the CTRL simulation, the soil moisture content at 5-cm depth at station EC was $0.23 \text{ m}^3 \text{ m}^{-3}$, whereas the initial value in the model was $0.6 \text{ m}^3 \text{ m}^{-3}$ (Fig. 4d). This large overestimate of the soil moisture content results in a continuing increase in the latent heat in the model (Figs. 4b, f). As a result, the near-surface in

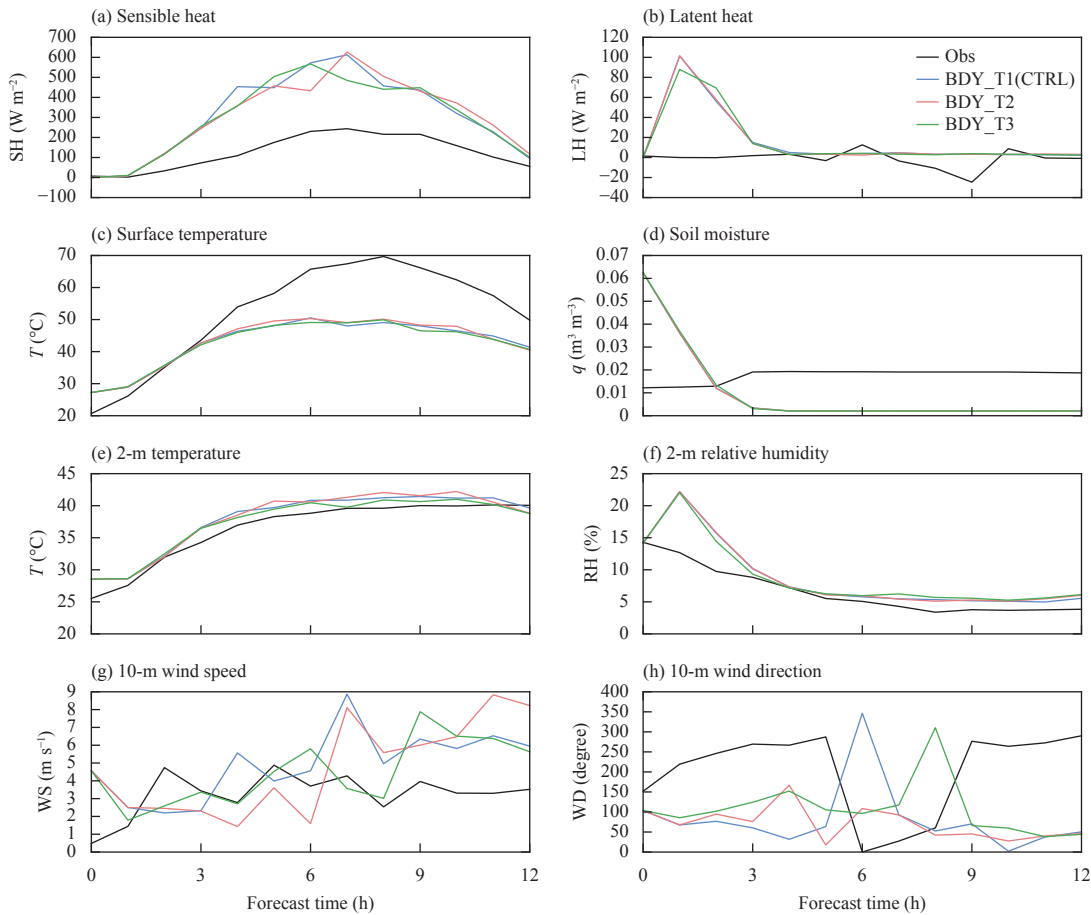


Fig. 4. Time series of the initial simulated surface variables from the innermost domain of the simulations and the surface observations at Tazhong station (39.03°N , 83.63°E) at 0800 BT 1 July 2016: (a) sensible heat flux, (b) latent heat flux, (c) surface temperature, (d) soil moisture content (q), (e) 2-m temperature, (f) 2-m relative humidity, (g) 10-m wind speed (WS), and (h) 10-m wind direction (WD).

Table 2. Summary of the verification of surface and air variables from 3 to 12 h for Tazhong station

Experiment	Sensible heat flux		Latent heat flux		Surface temperature		Soil moisture content		2-m temperature		2-m relative humidity		10-m wind speed	
	RMSE	BIAS	RMSE	BIAS	RMSE	BIAS	RMSE	Bias	RMSE	BIAS	RMSE	BIAS	RMSE	BIAS
CTRL	263.636	250.140	12.398	6.674	14.654	-13.373	0.017	-0.017	1.666	1.613	1.220	1.109	2.579	1.864
BDY_T2	249.395	240.660	12.383	6.253	14.116	-12.853	0.017	-0.017	1.912	1.817	1.275	1.162	2.943	1.307
BDY_T3	241.681	232.705	12.251	6.328	14.929	-13.737	0.017	-0.017	1.227	1.046	1.483	1.280	2.118	1.287
HFX_%75	151.119	134.594	12.544	6.354	14.740	-13.426	0.017	-0.017	3.078	3.016	0.956	0.826	3.335	0.874
HFX_%125	357.711	335.556	12.439	6.152	14.244	-13.043	0.017	-0.017	1.026	0.860	1.303	1.231	3.265	2.052
Noah	125.695	120.313	23.350	20.664	12.757	-11.502	0.048	0.048	1.046	0.983	10.116	9.904	2.788	1.795

the model is far moister than in the observations during the first few hours of model integration. The model has the ability to correct some of the bias due to the initial conditions of soil moisture and 2-m relative humidity from the CTRL experiment are closer to the observed values after 3 h of spin-up.

Figure 5 compares the potential temperatures (solid lines) simulated by the model with the GPS sounding measurements (dashed lines) at Tazhong from 0800 to 2000 BT 1 July 2016. The radiosonde is about 7 km away from Tazhong when it reached a height of 6 km. The profiles of the model simulations are therefore aver-

aged at a radius of 3.5 km from the measurement station. When the model is initialized at 0800 BT, the nocturnal inversion reaches 300 m (figure omitted). This inversion is eroded in the model by 1100 BT, in agreement with the observations, and both the model results and the observations reach about 300 m at 1100 BT (Fig. 5a). However, the simulated CBL grows faster in the morning than that in the observations due to a larger sensible heat flux, reaching 3500 m (3000 m in the observations) at 1400 BT (Fig. 5b). The simulated and observed CBL heights exceed 4000 and 5000 m, respectively, at 1700 BT (Fig. 5c). This indicates that the simulated CBL in-

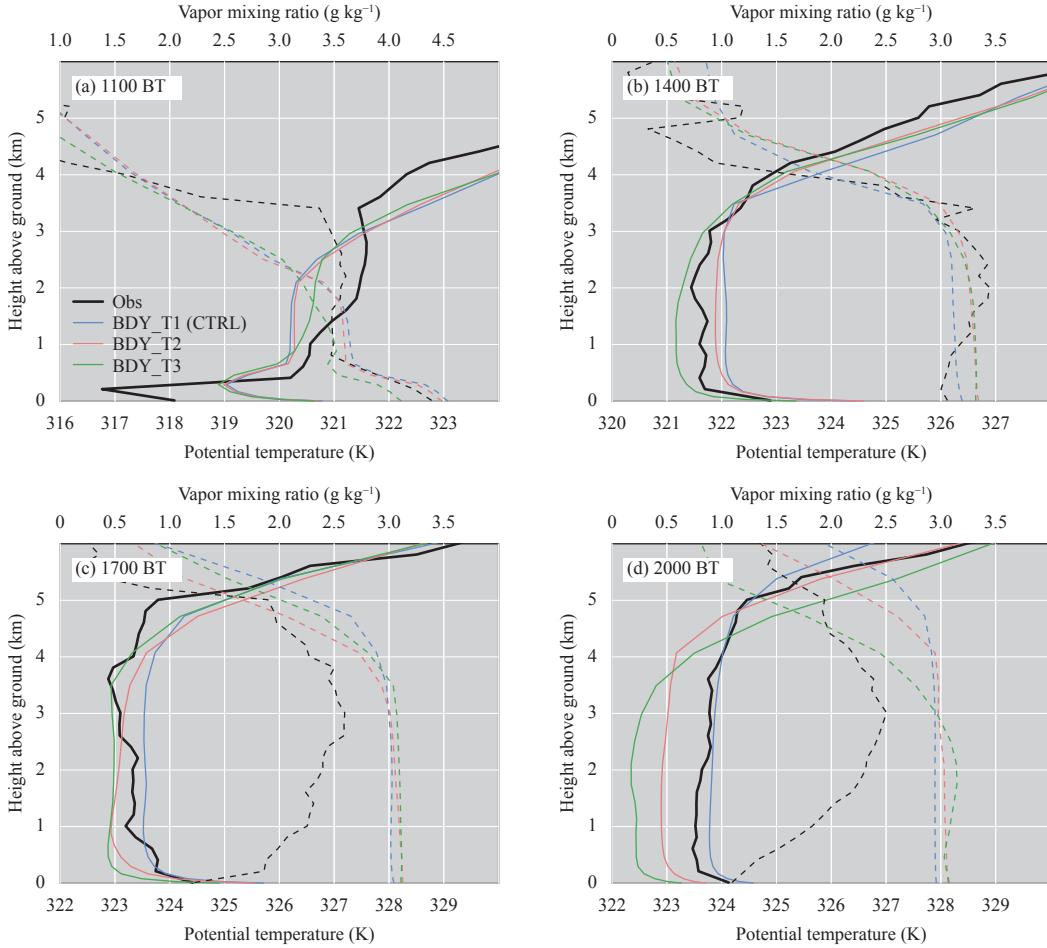


Fig. 5. Vertical profiles of the potential temperature (solid line; K) and vapor mixing ratio (dashed line; g kg^{-1}) from the innermost domain of the simulations and the observations from GPS sounding at Tazhong station ($39.03^\circ\text{N}, 83.63^\circ\text{E}$) at (a) 1100, (b) 1400, (c) 1700, and (d) 2000 BT 1 July 2016. The profiles of the model output are averaged over a radius of 3.5 km.

creases more slowly in the afternoon than the observed CBL. Compared with the measurements, the model is initially cooler, but with a faster heating rate in the morning. As a result, the model is warmer than the observations in the afternoon, but in agreement with the observations by the end of the day. This may be due to the differences in the potential temperature lapse rate above the top of the mixing layer between the observations and the simulated results. The stronger simulated inversion layer restricts the development of the CBL.

The model initially simulates a cooler and drier CBL at 1100 BT July 2016 than the observations (Fig. 5a). Compared with the observed potential temperature profile, the CBL appears earlier in model forecasts due to an obvious warming in the surface layer. The residual layer may play a key part in the deep PBL over the Taklimakan Desert. At 1100 BT, when the CBLH (Convective Boundary Layer Height) in the observations was about 300 m, the potential temperature was about 317 K in the PBL and 320 K in the residual layer. When the po-

tential temperature in the CBL increased to the value in the residual layer (320 K), the CBL merged with the residual layer and the height of the PBL in the observations reached 3000 m at 1400 BT. These results are in good agreement with those of Han et al. (2012), who, by analyzing observations from a CBL in the Badanjilin region, found that the CBL developed rapidly after 1200 LST, possibly as a result of the disappearance of the inversion layer.

When the sensible heat flux reached its maximum at 1400 BT (Fig. 5b), the potential temperature profile was closer to the observations than at the initial time and their value was higher than the observed values. By 2000 BT (Fig. 5d), the height of the CBL in the model reached its maximum value, consistent with the observations, despite being about 0.4 K cooler at lower levels (< 2.5 km). One cause of the higher temperatures produced in the model may be the large difference in the surface heat fluxes and we concluded that the surface sensible heat flux from the land surface parameterization was the cru-

cial factor affecting the CBL processes during the daytime in summer. Differences in the surface sensible heat flux create differences in the vertical development of the PBL. Thus, the large difference in the surface sensible heat flux between the model and the observations may lead to differences in the growth of the CBL during the daytime and in its peak depth during the simulation. Fortunately, the surface sensible heat flux computed by the land surface model can artificially be modified to control the calculation of the surface fluxes. Sensitive simulations will be realized and discussed in next section.

Figure 5 also shows vertical profiles of the vapor mixing ratio (dashed lines) at Tazhong station. The simulated profiles with a lower residual layer are much drier than the observations from 1500 to 3500 m at 1100 BT. Vertical mixing results in a uniform structure of the vapor mixing ratio within the CBL, so the differences between the profiles of the simulated results and the observations are remarkably reduced when the CBL is above 4000 m at 1400 BT. The differences are generally $< 1 \text{ g kg}^{-1}$ at 1100 BT, reaching a maximum of 0.3 g kg^{-1} at 1400 BT. However, the PBL shows an inverse layer at lower levels ($\leq 2000 \text{ m}$) with measured moisture content of $2.8\text{--}3.6 \text{ g kg}^{-1}$, which is not captured by the model. As the CBL grows, the inversion moisture structure below 3000 m develops and is maintained below 3000 m from 1400 to 2000 BT. By the end of the day, the simulated humidity of the CBL is higher than in the observations because the model cannot reproduce the inverse moisture layer within the CBL.

The inverse pattern in humidity may be caused by the interactions between the heterogeneous pattern of humidity and large-scale advection over the underlying surface. For instance, the interaction of an oasis with the desert environment may lead to an inverse humidity layer in the PBL above the desert. One possible reason for the discrepancy between the model results and the observations may be an error in the classification of land use type. The USGS land use data in the ARW-WRF model is based on Advanced Very High Resolution Radiometer 1-km resolution satellite data during 1992–93 and this land use data may no longer be accurate in the Taklimakan Desert. Misclassifications have also been found in the USGS land use data, which is the default land use dataset in the WRF model (Schicker et al., 2016). This is confirmed by the discrepancies in land use between the simulation and the observations at Tazhong station. The large-scale advection of dry air can affect the moisture profile. The moisture content is also variable in the horizontal direction, so advection at low levels may contribute to the

drier conditions in the lower PBL and more moist conditions in the upper PBL between 1100 and 2000 BT.

The mismatch between the model results and the observations in terms of moisture content suggest that the effects of land use type and large-scale advection need to be quantified and that more detailed data may be required for the Taklimakan Desert (both land and atmosphere) to realize more realistic results. Extra care should also be taken with the sparse and limited data at the periphery of the Taklimakan Desert (ter Maat et al., 2013).

3.2 Sensitivity to the lateral boundary conditions

After verifying the details of the LES experiments, we assessed the sensitivity of the simulations to the time resolution and domain size of the specified LBCs. For a one-way nest, the specified LBCs are obtained from coarser simulations. The analysis and forecast times from a previously run larger area simulation were used to specify the LBC. The primary cause of the differences in the structure of the PBL was diagnosed as the difference in the domain sizes and frequency provided by the coarser resolution. The aim was to assess the sensitivity of the finer LESs to uncertainties of the specified LBC forcing by model simulations with a larger area.

Figure 5 compares the profiles of the simulated potential temperature and vapor mixing ratio profiles from the LBC sensitivity experiments and observations. The results show that there is a distinct relationship between the development of the LBCs and the CBL. The profiles produced by the model are almost all the same at the initial time (figure omitted). However, the results show that there are large discrepancies in the CBL structure among the different experiments, and a larger domain size and higher time frequency for the LBCs leads to a warmer and drier PBL, but a cooler and moister free troposphere. This sensitivity is monotonic with respect to the LBCs (Fig. 5). Over the next three hours, the differences between the sensitivity experiments increase over time (Figs. 5a, b). The potential temperature profiles within the CBL diverge at 1100 BT. However, the results show a greater convergence in the afternoon as the CBL continues to grow (Fig. 5c), but the largest discrepancies are found at end of the day (Fig. 5d) when the model CBL potential temperature is warmer than the observations by up to 0.7 and 0.9 K in BDY_T2 and BDY_T1, respectively.

Figure 6 shows cross-sections of the horizontal winds along 39.03°N , superposed with the potential temperature and vapor mixing ratio. Less frequent updates of the LBCs are desirable in the cold zone near the LBCs, which results in cold advection of the temperature and

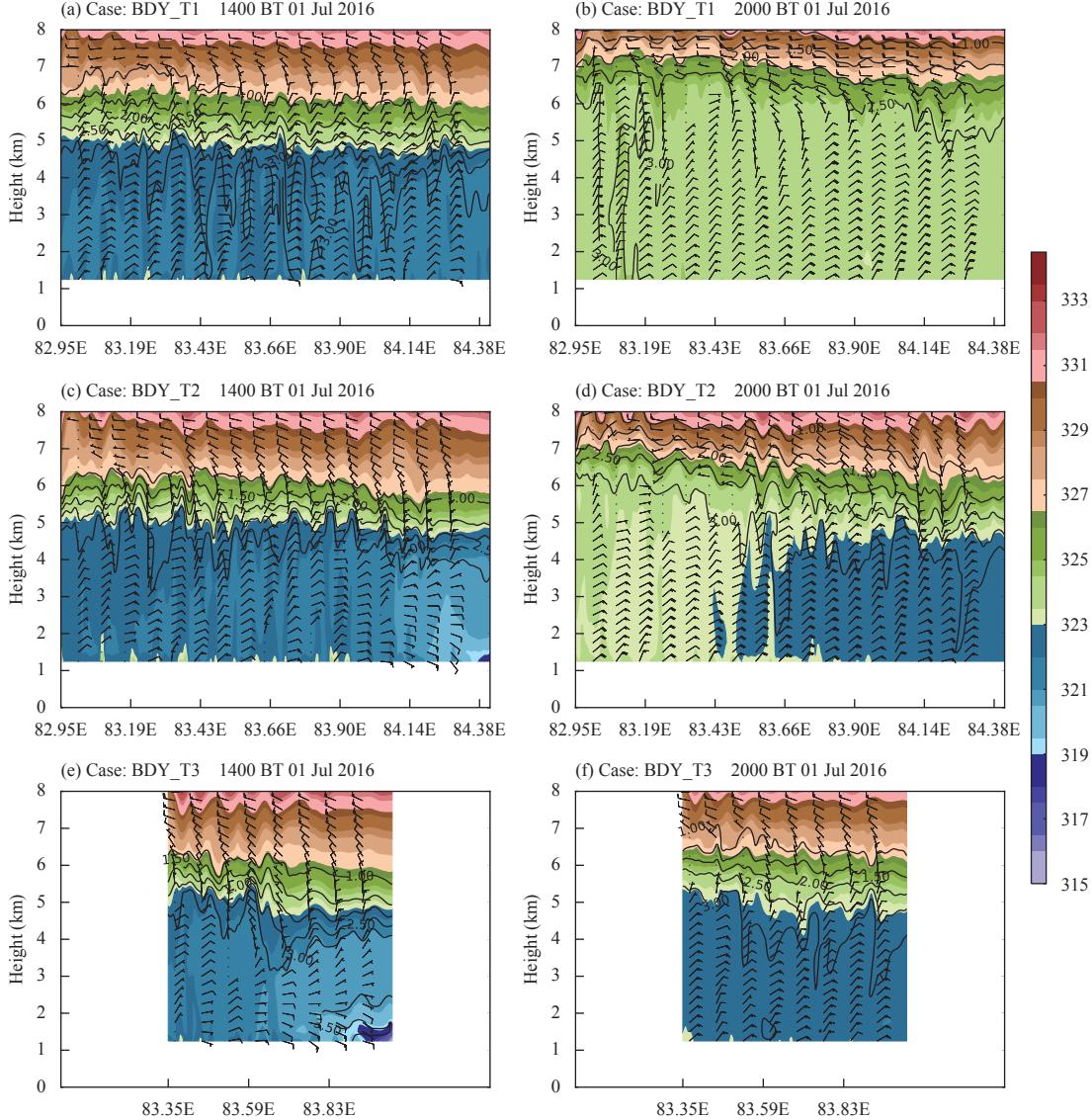


Fig. 6. Cross-sections along 39.03°N of the horizontal winds (barbs; m s^{-1}) at intervals of 5 m s^{-1} superposed with the potential temperature (shaded; K) and vapor mixing ratio (contours; g kg^{-1}) from (a, b) BDY_T1, (c, d) BDY_T2, and (e, f) BDY_T3 experiments at (a, c, e) 1400 and (b, d, f) 2000 BT 1 July 2016.

moisture to the area of interest (Figs. 6b, c). A larger domain size, which changes the distance of the area of interest from the LBC, is efficient in reducing the influence of large forecast errors near the LBCs on the area of interest (Figs. 6a, c).

To further examine the impact of the LBCs on the turbulence in the deep Taklimakan Desert CBL, the instantaneous vertical velocity fields are shown in Fig. 7. By 1400 BT, the convection of the CTRL simulation had clearly intensified under strong surface heating (Xu et al., 2018). Thus, the maximum vertical velocity reached 9 m s^{-1} and the depth of the mixed layer grew to about 4.3 km (Fig. 7a). The distances between the boundary layer rolls correspondingly increased to about 12 km and the height

of the peak up-draft was raised to just under 4 km. The cellular shape of the up- and down-drafts characteristic of the boundary layer rolls is clear in the horizontal view showing the strength of convection. The BDY_T2 and BDY_T3 experiments (Figs. 7b, c) both reproduce motions with much weaker maximum and minimum values at the boundary of the domain. In BDY_T3, Tazhong station at the center of the model is directly influenced by the inflow of cold advection produced by the low-frequency LBCs, resulting in much weaker maximum and minimum values of w (about 6 m s^{-1}). However, despite the underestimation of the potential temperature, the w fields in the BDY_T2 experiment are similar to those in the CTRL experiment in plan view and the horizontal ex-

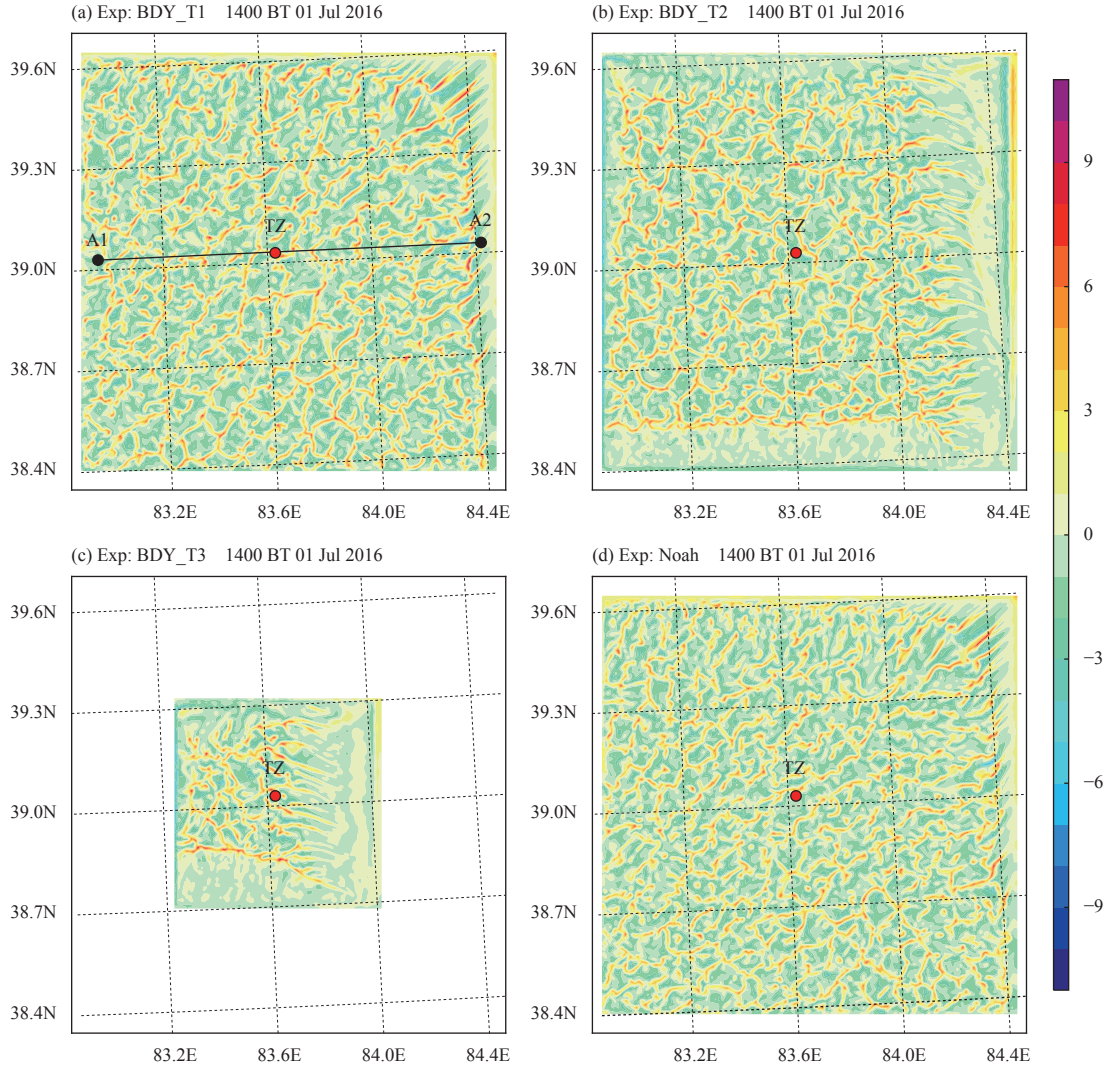


Fig. 7. Instantaneous vertical velocity fields (shading; m s^{-1}) at 3000 m for the (a) BDY_T1 (CTRL), (b) BDY_T2, (c) BDY_T3, and (d) Noah experiments at 1400 BT 1 July 2016.

tent of the up-/down-drafts agrees with the CTRL experiment.

To further examine the vertical structure of the desert CBL, Fig. 8 presents vertical cross-sections of w along Tazhong station (39°N). Wide and regularly spaced updrafts along A1–A2 split into stronger and more irregular motions in the CTRL and BDY_T2 experiments. The up-drafts are much weaker in experiment BDY_T3 (Fig. 8c). The peak up-drafts in BDY_T3 are about 4 m s^{-1} , much weaker than in the CTRL (9 m s^{-1}) and BDY_T2 (8 m s^{-1}) experiments. The inflow boundary is wider in BDY_T2 and BDY_T3 and the intensity of the convection is weaker at the boundary. The horizontal distribution of the vertical velocity at Tazhong station in BDY_T3 is much weaker than in BDY_T2. The results suggest that the model results are sensitive to changes in the time resolution and domain size of the specified

LBCs. The mismatch among sensitive experiments means that the effect of the LBCs needs to be quantified to realize a more realistic performance in sub-kilometer-scale simulations.

3.3 Simulations with different surface sensible heat fluxes and land surface models

An important cause of the differences in the structure of the PBL was determined to be the differences in sensible heat flux predicted by the land surface schemes. The sensible heat flux is a key factor affecting the height of the CBL during daytime in summer. The difference between the models and observations may therefore lead to differences in the growth of the PBL during the day. To further confirm whether this occurs, three additional sensitive simulations were realized based on the CTRL experiment. The Noah land surface model replaced the

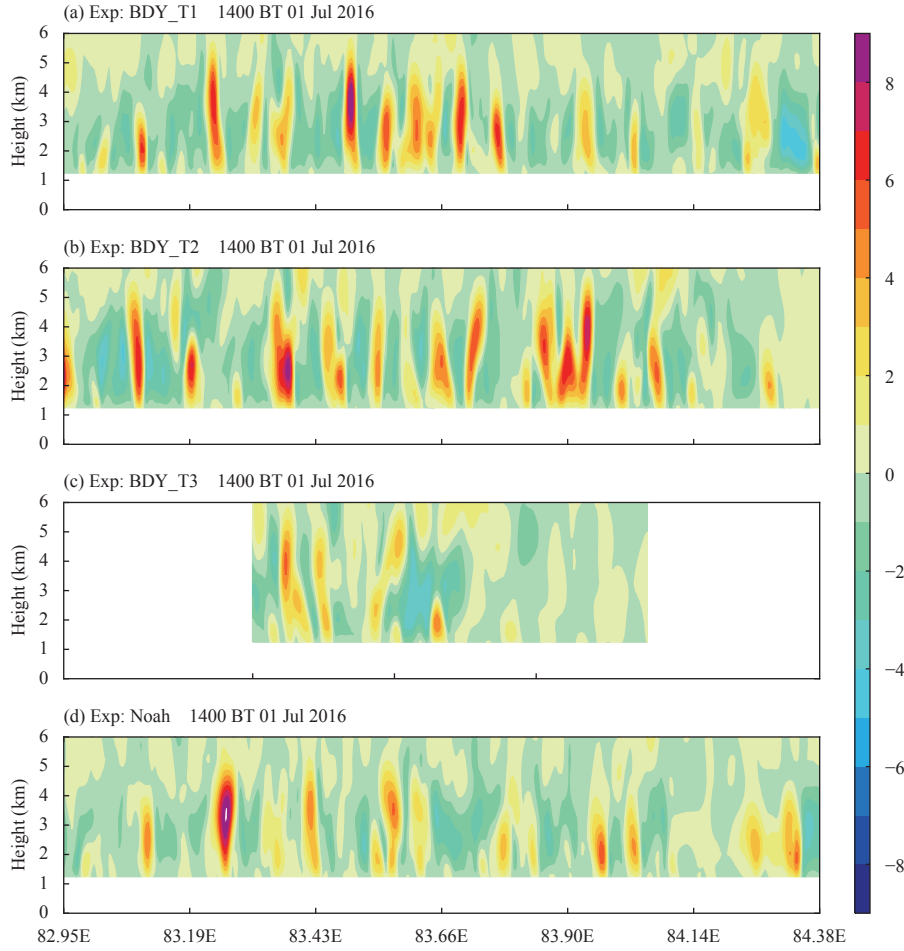


Fig. 8. Vertical cross-sections of the instantaneous vertical velocity fields (shading; m s^{-1}) along A1–A2 in for the (a) BDY_T1 (CTRL), (b) BDY_T2, (c) BDY_T3, and (d) Noah experiments at 1400 BT 1 July 2016.

RUC land surface model in the CTRL experiment and the sensible heat fluxes for HFX-125% and HFX-75% are 125% and 75% that of the CTRL (HFX-100%) experiment while the other parameters remain the same.

The results in Fig. 9 and Table 2 show that HFX-75% successively improved the simulation of the sensible heat flux with an RMSE of 151 compared with 263 and 357 in the CTRL and HFX-125% experiments, respectively. The Noah land surface experiment yielded the best performance in terms of the sensible heat flux, surface temperature, and air temperature. However, the Noah land surface model showed large discrepancies with the observations in terms of the soil moisture content, resulting in a dramatic overestimate of the latent heat flux and relative humidity compared with the CTRL experiment.

A further examination of the potential temperature and vapor mixing ratio (Fig. 10) indicates that a smaller sensible heat flux leads to a cooler, moister lower PBL and a warmer, drier free atmosphere. This sensitivity is monotonic with respect to the sensible heat flux. The structure of the CBL from the HFX-75% and Noah experiments

matches the GPS radiosonde measurements better than the CTRL (HFX-100%) simulations. The potential temperature profiles from the CTRL (HFX-100%) and HFX-125% experiments are consistently warmer than the observations by about 0.4 and 0.5 K, respectively, whereas the results from the HFX-75% and Noah experiments are within about 0.2 K at 1400 BT (Fig. 10b). These results suggest that the model is sensitive to changes in the sensible heat flux from the land surface model. The simulations converge at the end of the day, although there are still differences at 2000 BT (Fig. 10d). The HFX-75% and Noah experiments with a weaker surface sensible heat flux still produce almost the same deep CBL as the CTRL and HFX-125% experiments. This indicates that the sensible heat flux may not the dominant factor in the formation of the deep CBL over the Taklimakan Desert.

The results of the simulations of the desert PBL in the morning agree with previous studies of the sensitivities the land surface model in other areas (Hu et al., 2010; Zhang et al., 2017). However, all the experiments produce nearly the same height of the CBL and moisture

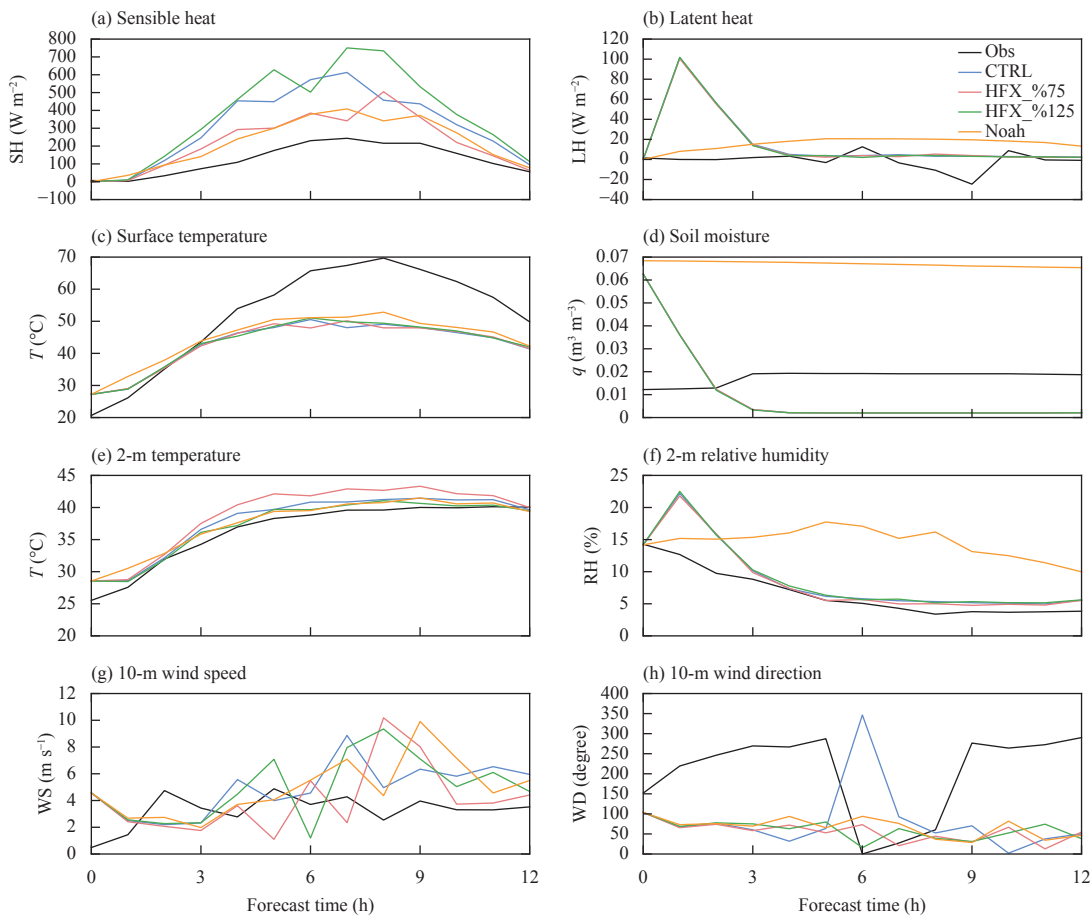


Fig. 9. Time series of the initial simulated surface variables for the sensible heat flux sensitivity and Noah land surface experiments: (a) sensible heat flux, (b) latent heat flux, (c) surface temperature, (d) soil moisture content (q), (e) 2-m temperature, (f) 2-m relative humidity, (g) 10-m wind speed (WS), and (h) 10-m wind direction (WD).

content from 1700 to 2000 BT 1 July 2016 (Figs. 10b, d), in agreement with the observations in the PBL. The effects of the sensible heat flux on the evolution of the PBL structures in the Taklimakan Desert during this period need to be examined further to determine why the simulations are insensitive to land surface processes at the end of the day. As reported by Stull (1988), the development of the CBL is mainly influenced by the effects of thermodynamic and turbulent entrainment if we do not consider factors such as large-scale advection or subsidence. In addition to the surface sensible heat, the intensity of the entrainment process determines the increase in the CBL. Thus, the entrainment rate w_e is a valuable indicator of the development of the structure of the PBL. The rate of growth of the CBL is mainly determined by w_e at the inversion layer without large-scale vertical motion. The variable w_e usually has a positive correlation with the amount of heat flux at the inversion layer ($\overline{w'\theta'_v}_h$), and LES experiments show that $\overline{w'\theta'_v}_h$ is about -0.2 times as much as the surface flux of the buoyancy ($\overline{w'\theta'_0}$). From 1100 to 1400 BT, a larger sensible heat flux is clearly

correlated with stronger turbulent entrainment and warmer air from the free atmosphere entraining into the mixing layer (ML). As a result, the CBL develops rapidly and warms too quickly in the early simulation phase due to the clear increase in temperature and strong vertical mixing in the model. The reduction in the sensible heat flux reproduces the evolution of the desert PBL better in the early simulation phase because the HFX-75% and Noah simulations produce the smallest simulation errors in both temperature and moisture. However, the height of the CBL and the potential temperature for HFX-75% and Noah reach > 5000 m and 323.2 K, respectively, at 1700 BT (Fig. 10a). For the rest of the day, the rate of increase in the height of the CBL slows due to the deep CBL (> 5000 m), which requires more heat for the increase in the depth of the PBL. The variable w_e decreases with increasing intensity of the inversion, which inhibits the mixing and entrainment processes. These two factors limit the growth of the CBL when the height is > 5000 m in this deep desert event. Therefore, increasing the sensible heat flux from 75% to 125% significantly re-

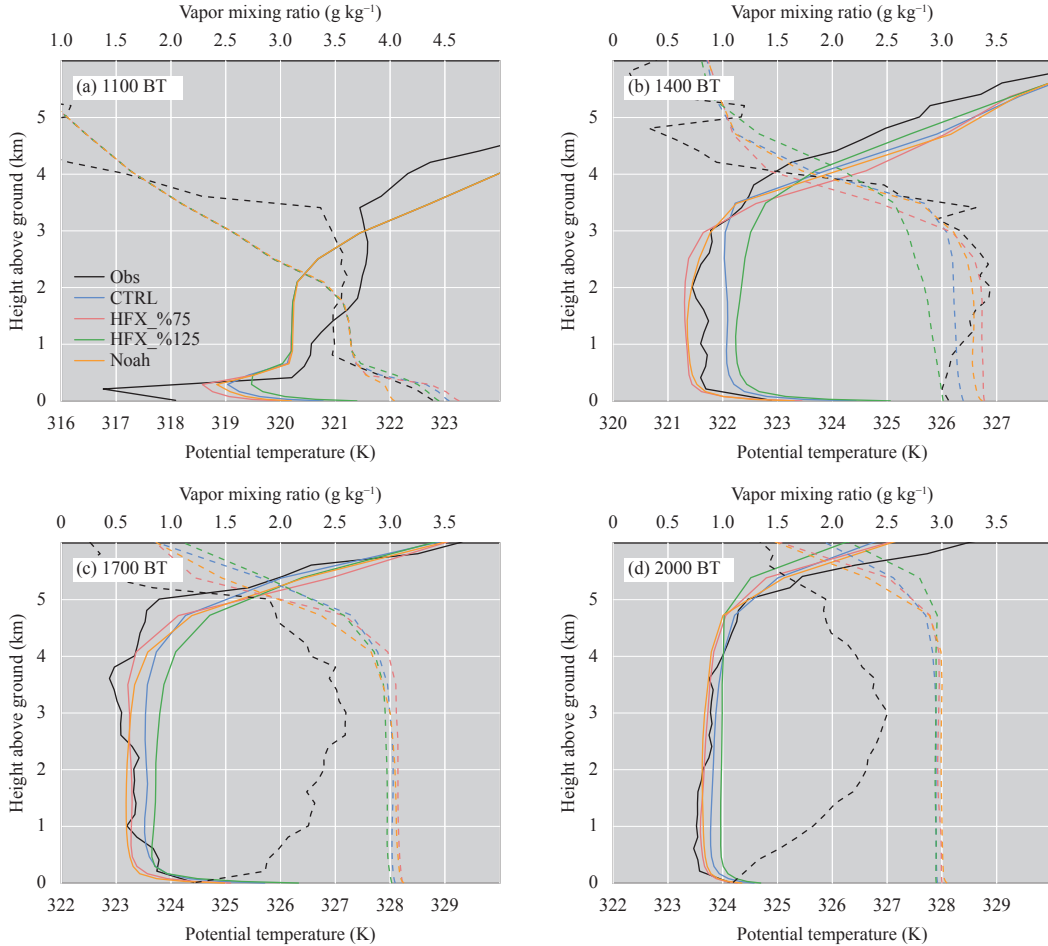


Fig. 10. Vertical profiles of the potential temperature (solid line; K) and vapor mixing ratio (dashed line; g kg^{-1}) for the sensible heat flux sensitivity and Noah land surface experiments at (a) 1100, (b) 1400, (c) 1700, and (d) 2000 BT 1 July 2016. The profiles of the model output are averaged over a radius of 3.5 km.

duced the total time required for the increase in the CBL to a relatively low altitude (< 5000 m) at the middle and preliminary stages of the development of the CBL, rather than produces a higher CBL at a later stage. When the height of the CBL over the Taklimakan Desert exceeds 5000 m, it may not change in proportion to the sensible heat flux (Fig. 10d). As a result, the PBL is basically the same in the WRF simulations and is not sensitive to the sensible heat flux at the end of the day.

4. Summary

In this paper, we assessed the performance of the WRF model LES in an example of a deep convective PBL over the Taklimakan Desert. The tests were performed with multiple configurations and sensitivity experiments. The sensitivity tests for the LBCs showed that the model results are sensitive to changes in the size of the time resolution and domain of the specified LBC. A larger domain size changes the distance of the area of in-

terest from the LBC and is efficient in reducing the influence of the large forecast error near the LBC.

The model reproduces the evolution of PBL processes reasonably well with the configuration used in this study. The model shows discrepancies between the main CBL characteristics in the morning, including the thermal and moisture structures. The model simulates the relatively colder and drier morning CBL, underestimating the temperature in the near-surface layer at Tazhong station by up to 1.5 K and the moisture content by 1 g kg^{-1} . The overestimation of the CBL profile may be caused by initial discrepancies between the model and the observations. This indicates that the results are sensitive to the initial conditions of the model. However, the simulation seems to be able to correct some of the moisture bias due to the large bias of soil moisture. The model correctly reproduces the thermal structure in the afternoon, but the simulations are relatively warmer and moister than the observations. The potential temperature profile at the CBL appears warmer than the observations by about 0.4

K. The model seriously overestimates the moisture content in the afternoon and overestimates the vapor mixing ratio in the CBL by about $1\text{--}2 \text{ g kg}^{-1}$. The largest discrepancies are found in 0–3-km layer, where the model vapor mixing ratio is twice as moist as that of the observations (up to about 3 g kg^{-1}).

Three additional simulations were carried out to find out whether the large differences in the sensible heat flux lead to differences in growth of the CBL during the daytime relative to the CTRL experiment. The results suggest that the model results are sensitive to changes in the sensible heat flux and different land surface models. The large difference between the model and observations may lead to differences in the growth of the CBL during the daytime. It was concluded the surface sensible heat flux is an important factor affecting the processes of the CBL over the Taklimakan Desert during the daytime in summer. However, its peak depth during the simulation was less sensitive to the sensible heat flux because w_e had decreased by the end of the day. One should note that the CBL of Taklimakan need several days of favorable environment to reach its super depth ($> 4000 \text{ m}$), and sustained high temperature and SH is the crucial factor for CBL to develop from shallow to deep CBL. The SH is not dominant factor, but still an important factor affecting the deep CBL.

Future work will study several other examples of a deep CBL over the Taklimakan Desert to determine their common features. We hope to use high-resolution models and observations to describe the fine characteristics of a typical deep CBL over the Taklimakan Desert, particularly the turbulent and vertical mixing and its impact on the regional weather forecast. This research aims to improve our understanding of the deep CBL over the Taklimakan Desert and its influence on the regional weather and climate.

Acknowledgments. The author thanks the reviewers and editors for their professional advice in improving this paper.

REFERENCES

- Chen, F., and J. Dudhia, 2001a: Coupling an advanced land surface-hydrology model with the Penn State-NCAR MM5 modeling system. Part II: Preliminary model validation. *Mon. Wea. Rev.*, **129**, 587–604, doi: 10.1175/1520-0493(2001)129<0587:CAALSH>2.0.CO;2.
- Chen, F., and J. Dudhia, 2001b: Coupling an advanced land surface-hydrology model with the Penn State-NCAR MM5 modeling system. Part I: Model implementation and sensitivity. *Mon. Wea. Rev.*, **129**, 569–585, doi: 10.1175/1520-0493(2001)129<0569:CAALSH>2.0.CO;2.
- Dudhia, J., 1989: Numerical study of convection observed during the winter monsoon experiment using a mesoscale two-dimensional model. *J. Atmos. Sci.*, **46**, 3077–3107, doi: 10.1175/1520-0469(1989)046<3077:NSOCOD>2.0.CO;2.
- Engelstaedter, S., R. Washington, C. Flamant, et al., 2015: The Saharan heat low and moisture transport pathways in the central Sahara—Multaircraft observations and Africa-LAM evaluation. *J. Geophys. Res. Atmos.*, **120**, 4417–4442, doi: 10.1002/2015JD023123.
- Garcia-Carreras, L., D. J. Parker, J. H. Marsham, et al., 2015: The turbulent structure and diurnal growth of the Saharan atmospheric boundary layer. *J. Atmos. Sci.*, **72**, 693–713, doi: 10.1175/JAS-D-13-0384.1.
- Han, B., S. H. Lyu, and Y. H. Ao, 2012: Development of the convective boundary layer capping with a thick neutral layer in Badanjilin: Observations and simulations. *Adv. Atmos. Sci.*, **29**, 177–192, doi: 10.1007/s00376-011-0207-4.
- Heinold, B., P. Knippertz, and J. H. Marsham, 2013: Large eddy simulations of nocturnal low-level jets over desert regions and implications for dust emission. EGU General Assembly 2013 Vienna, Austria, 7–12 April, EGU.
- Heinold, B., P. Knippertz, and R. J. Beare, 2015: Idealized large-eddy simulations of nocturnal low-level jets over subtropical desert regions and implications for dust-generating winds. *Quart. J. Roy. Meteor. Soc.*, **141**, 1740–1752, doi: 10.1002/qj.2475.
- Heinze, R., D. Mironov, and S. Raasch, 2015: Second-moment budgets in cloud topped boundary layers: A large-eddy simulation study. *J. Adv. Model. Earth Syst.*, **7**, 510–536, doi: 10.1002/2014MS000376.
- Hong, S. Y., and H. L. Pan, 1996: Nonlocal boundary layer vertical diffusion in a medium-range forecast model. *Mon. Wea. Rev.*, **124**, 2322–2339, doi: 10.1175/1520-0493(1996)124<2322:NBLVDI>2.0.CO;2.
- Hong, S. Y., and J. O. J. Lim, 2006: The WRF single-moment 6-class microphysics scheme (WSM6). *Asia-Pacific J. Atmos. Sci.*, **42**, 129–151.
- Hu, X.-M., J. W. Nielsen-Gammon, and F. Q. Zhang, 2010: Evaluation of three planetary boundary layer schemes in the WRF model. *J. Appl. Meteor. Climatol.*, **49**, 1831–1844, doi: 10.1175/2010JAMC2432.1.
- Kain, J. S., and J. M. Fritsch, 1993: Convective parameterization for mesoscale models: The Kain-Fritsch scheme. *The Representation of Cumulus Convection in Numerical Models*, Emanuel, K. A., and D. J. Raymond, Eds., American Meteorological Society, Boston, MA, 165–170, doi: 10.1007/978-1-935704-13-3_16.
- Kain, J. S., 2004: The Kain-Fritsch convective parameterization: An update. *J. Appl. Meteor.*, **43**, 170–181, doi: 10.1175/1520-0450(2004)043<0170:TKCPAU>2.0.CO;2.
- LeMone, M. A., M. Tewari, F. Chen, et al., 2013: Objectively determined fair-weather CBL depths in the ARW-WRF model and their comparison to CASES-97 observations. *Mon. Wea. Rev.*, **141**, 30–54, doi: 10.1175/MWR-D-12-00106.1.
- Liu, Y. B., T. Warner, Y. W. Liu, et al., 2011: Simultaneous nested modeling from the synoptic scale to the LES scale for wind energy applications. *J. Wind Eng. Ind. Aerod.*, **99**, 308–319, doi: 10.1016/j.jweia.2011.01.013.
- Liu, Y. Q., Q. He, H. S. Zhang, et al., 2012: Improving the CoLM

- in Taklimakan Desert hinterland with accurate key parameters and an appropriate parameterization scheme. *Adv. Atmos. Sci.*, **29**, 381–390, doi: 10.1007/s00376-011-1068-6.
- Marsham, J. H., P. Knippertz, N. S. Dixon, et al., 2011: The importance of the representation of deep convection for modeled dust-generating winds over West Africa during summer. *Geophys. Res. Lett.*, **38**, L16803, doi: 10.1029/2011GL048368.
- Mlawer, E. J., S. J. Taubman, P. D. Brown, et al., 1997: Radiative transfer for inhomogeneous atmospheres: RRTM, a validated correlated-k model for the longwave. *J. Geophys. Res. Atmos.*, **102**, 16663–16682, doi: 10.1029/97JD00237.
- Moeng, C. H., J. Dudhia, J. Klemp, et al., 2007: Examining two-way grid nesting for large eddy simulation of the PBL using the WRF model. *Mon. Wea. Rev.*, **135**, 2295–2311, doi: 10.1175/MWR3406.1.
- National Centers for Environmental Prediction, National Weather Service, NOAA, et al., 2015: NCEP GDAS/FNL 0.25 Degree Global Tropospheric Analyses and Forecast Grids. Research Data Archive at the National Center for Atmospheric Research. *Computational and Information Systems Laboratory* doi: 10.5065/D65D8PKW.
- Rai, R. K., L. K. Berg, B. Kosović, et al., 2017: Comparison of measured and numerically simulated turbulence statistics in a convective boundary layer over complex terrain. *Bound.-Layer Meteor.*, **163**, 69–89, doi: 10.1007/s10546-016-0217-y.
- Schicker, I., D. Arnold Arias, and P. Seibert, 2016: Influences of updated land-use datasets on WRF simulations for two Austrian regions. *Meteor. Atmos. Phys.*, **128**, 279–301, doi: 10.1007/s00703-015-0416-y.
- Shin, H. H., and S. Y. Hong, 2011: Intercomparison of planetary boundary-layer parametrizations in the WRF Model for a single day from CASES-99. *Bound.-Layer Meteor.*, **139**, 261–281, doi: 10.1007/s10546-010-9583-z.
- Shin, H. H., and S. Y. Hong, 2015: Representation of the subgrid-scale turbulent transport in convective boundary layers at gray-zone resolutions. *Mon. Wea. Rev.*, **143**, 250–271, doi: 10.1175/MWR-D-14-00116.1.
- Skamarock, W. C., J. B. Klemp, J. Dudhia, et al., 2008: A Description of the Advanced Research WRF Version 3. NCAR Technical Note, NCAR/TN-475+STR, National Center for Atmospheric Research, Boulder, Colorado, USA, doi: 10.5065/D68S4MVH.
- Smirnova, T. G., J. M. Brown, and S. G. Benjamin, 1997: Performance of different soil model configurations in simulating ground surface temperature and surface fluxes. *Mon. Wea. Rev.*, **125**, 1870–1884, doi: 10.1175/1520-0493(1997)125<1870:PODSMC>2.0.CO;2.
- Smirnova, T. G., J. M. Brown, S. G. Benjamin, et al., 2000: Parameterization of cold-season processes in the MAPS land-surface scheme. *J. Geophys. Res. Atmos.*, **105**, 4077–4086, doi: 10.1029/1999JD901047.
- Stull, R. B., 1988: *An Introduction to Boundary Layer Meteorology*. Atmospheric Sciences Library, Dordrecht, Boston, 89.
- Sun, J. N., and Q. J. Xu, 2009: Parameterization of sheared convective entrainment in the first-order jump model: Evaluation through large-eddy simulation. *Bound.-Layer Meteor.*, **132**, 279–288, doi: 10.1007/s10546-009-9394-2.
- Talbot, C., E. Bou-Zeid, and J. Smith, 2012: Nested mesoscale large-eddy simulations with WRF: Performance in real test cases. *J. Hydrometeorol.*, **13**, 1421–1441, doi: 10.1175/JHM-D-11-048.1.
- ter Maat, H. W., E. J. Moors, R. W. A. Hutjes, et al., 2013: Exploring the impact of land cover and topography on rainfall maxima in the Netherlands. *J. Hydrometeorol.*, **14**, 524–542, doi: 10.1175/JHM-D-12-036.1.
- Wang, M. Z., W. S. Wei, Q. He, et al., 2016a: Summer atmospheric boundary layer structure in the hinterland of Taklimakan Desert, China. *J. Arid Land*, **8**, 846–860, doi: 10.1007/s40333-016-0054-3.
- Wang, M. Z., H. Lu, H. Ming, et al., 2016b: Vertical structure of summer clear-sky atmospheric boundary layer over the hinterland and southern margin of Taklamakan Desert. *Meteor. Appl.*, **23**, 438–447, doi: 10.1002/met.1568.
- Zhang, F. M., Z. X. Pu, and C. H. Wang, 2017: Effects of boundary layer vertical mixing on the evolution of hurricanes over land. *Mon. Wea. Rev.*, **145**, 2343–2361, doi: 10.1175/MWR-D-16-0421.1.